The Predictive Power of Computational Astrophysics as a Discovery Tool
Proceedings IAU Symposium No. 362, 2023
D. Bisikalo, D. Wiebe & C. Boily, eds.
doi:10.1017/S174392132200165X

Interplay of various particle acceleration processes in astrophysical environment

Sayan Kundu* **and Bhargav Vaidya**

Department of Astronomy, Astrophysics and Space Engineering
Indian Institute of Technology, Indore
Madhya Pradesh, India - 452020
*sayan.astronomy@gmail.com

Abstract. Astrophysical systems possess various sites of particle acceleration, which gives rise to the observed non-thermal spectra. Diffusive shock acceleration (DSA) and stochastic turbulent acceleration (STA) are the candidates for producing very high energy particles in weakly magnetized regions. While DSA is a systematic acceleration process, STA is a random energization process, usually modelled as a biased random walk in energy space with a Fokker-Planck equation. In astrophysical systems, different acceleration processes work in an integrated manner along with various energy losses.

Here we study the interplay of both STA and DSA in addition to various energy losses, in a simulated RMHD jet cocoon. Further, we consider a phenomenologically motivated STA timescale and discuss its effect on the emission profile of the RMHD jet. A parametric study on the turbulent acceleration timescale is also conducted to showcase the effect of turbulence damping on the emission structure of the simulated jet.

Keywords. Acceleration of particles, Radiation mechanisms: nonthermal, Plasmas, Turbulence

1. Introduction

Particle acceleration is an ubiquitous phenomenon in astrophysical environments. It presents a possible reason for the observed abundance of non-thermal particles and their spatial distribution throughout the source in various extra-galactic systems, thus explaining the observed emission signatures from these sources. The existing literature (Blandford 1994; Marcowith et al. 2020) suggests three main mechanisms to energize charged particles in various astrophysical plasma environments: diffusive shock acceleration (DSA), coherent electric field acceleration due to reconnection, and stochastic turbulent acceleration (STA). Among these, DSA and STA are plausible mechanisms for accelerating charged particles in weakly magnetized medium and magnetic reconnection is more efficient in accelerating particles in magnetically dominated systems. Since Fermi (1949), magneto-hydrodynamic turbulence is known to be an important source for accelerating particles through STA, while DSA requires shocks to be present in the system. Even-though, comparing by the acceleration timescale, DSA is more efficient, STA, however, has been invoked to explain the particle acceleration processes in various astrophysical systems (see for example, Petrosian 2012; Vurm & Poutanen 2009; Ferrand & Marcowith 2010; Schlickeiser & Dermer 2000; Asano & Hayashida 2018; O'Sullivan, Reville, & Taylor 2009; Fan et al. 2008; Donnert & Brunetti 2014).

Incorporating these particle acceleration processes in large-scale numerical simulations is an area of active research (Hanasz, Strong, & Girichidis 2021; Vazza et al. 2021;

Donnert & Brunetti 2014) and recently higher order numerical schemes are being developed in this regard (Kundu, Vaidya, & Mignone 2021; Winner et al. 2019). Considering the length-scale constraint of numerical simulations, multi-scale realistic astrophysical simulations demand various micro-physical quantities, such as viscosity, various acceleration timescale, resistivity, damping rate of turbulence etc., to be calculated apriori and fed into the simulation as an input. This poses a problem, as apriori calculation of the micro-physical quantities in such complex environments is very difficult. So in the present work, we choose a phenomenologically motivated timescale for stochastic acceleration considering the micro-physics of turbulence damping phenomena, observed in real astrophysical scenarios, and show the interplay of STA and DSA on the emission profile of a simulated toy RMHD jet. We also performed a parametric study on the new timescale and analyze its effect on the emission structure.

2. Stochastic Turbulent Acceleration

Due to random scattering, between charged particles and various MHD waves in a magnetized environment the charged particle or cosmic ray distribution follows a Fokker-Planck equation in momentum space (Webb 1989; Vaidya et al. 2018; Kundu, Vaidya, & Mignone 2021),

$$\frac{\partial \chi_p}{\partial \tau} + \frac{\partial}{\partial \gamma}\left[(S + D_A)\chi_p\right] = \frac{\partial}{\partial \gamma}\left(D\frac{\partial \chi_p}{\partial \gamma}\right) , \tag{2.1}$$

where, τ is the proper time, $\gamma \approx p/m_0 c$ is the Lorentz factor of the cosmic ray, with m_0 being the mass of the cosmic ray particle and c is the speed of light in vacuum, $\chi_p = N/n$, with $N(p, \tau)$ being the number density of the non-thermal particles with momentum between p and $p + dp$ and n being the number density of the fluid at the position of the macro-particle, S corresponds to various radiative and adiabatic losses; $D_A = 2D/\gamma$ corresponds to the acceleration due to Fermi II order with D being the diffusion coefficient.

2.1. *Modelling momentum diffusion coefficient*

All the micro-physical processes of the random scattering phenomena are contained in the momentum diffusion coefficient D of Eq. (2.1). Even-though the mathematical form of this diffusion coefficient, due to interactions of cosmic ray with turbulent magnetized medium, have analytically been derived (see, for instance, Schlickeiser 2002; Brunetti & Lazarian 2007; O'Sullivan, Reville, & Taylor 2009) for specific turbulent cases, a general form is still lacking. Due to this reason we choose a parametrized acceleration timescale for our simulations,

$$t_A = \tau_A \exp\{\tau/\tau_d\} \tag{2.2}$$

where, t_A is the acceleration timescale, τ_A, τ_d are some arbitrary parameters and τ is time. The motivation for choosing such kind of acceleration timescale is the finite energy constraint, which implies that, in realistic situations the amount of energy, which could be channelled to the non-thermal particles due to turbulence, is limited and particles can not get accelerated forever. So for a realistic scenario one should consider the effect of damping of the turbulence in the system, which has been taken care of by the presence of the exponential term in t_A. Time-exponential decay in the charged particles' velocity-velocity correlation, for spatial diffusion coefficient, or in the pitch angle auto-correlation has already been reported by various authors (see for example Fraschetti & Giacalone 2012, and the references therein), we have prescribed an extension of such formalism for

https://doi.org/10.1017/S174392132200165X Published online by Cambridge University Press

the momentum diffusion scenario. The momentum diffusion coefficient D, related to the acceleration timescale, therefore becomes,

$$D = \frac{\gamma^q}{2t_A} = \frac{\gamma^q}{2\tau_A} \exp\left\{-\frac{\tau}{\tau_d}\right\}, \tag{2.3}$$

where q is the exponent and for all our simulations we assume $q = 2$.

2.2. *Numerical Algorithm*

In this work, we use a finite volume relativistic magneto-hydrodynamic code PLUTO (Mignone et al. 2007) to do the simulations and also utilize the Lagrangian particle module (Mukherjee et al. 2021; Vaidya et al. 2018) to analyze the emission signatures of the simulated structure. The Lagrangian particle module employs a 2^{nd} order accurate conservative RK-IMEX scheme (Kundu, Vaidya, & Mignone 2021) to solve Eq. (2.1). For this work, we modified the scheme considering the fact that due to various cooling processes, the particle spectrum falls off very rapidly in the higher γ region. Thus, following Winner et al. (2019) we floor the spectrum after a certain threshold χ_{cut} and treat the numerical values below it as zeros. Further note that, the flooring of the particle spectra is done to only those macro-particles which has encountered at least one shock. Moreover, for all our simulations we consider $\chi_{cut} = 10^{-21}$ and the value of CFL number is 0.8 while solving Eq. (2.1).

3. Numerical Setup

We choose to simulate an axisymmetric RMHD jet as a toy model to analyze the interplay of various particle acceleration processes and its effect on the emission signatures. The simulation is performed with a unit length of $\hat{L}_0 = 100\,\mathrm{pc}$, unit density of $\hat{\rho}_0 = 1.67 \times 10^{-24}\,\mathrm{gr\,cm^{-3}}$ and a unit velocity of $\hat{v}_0 = c = 3 \times 10^{10}\,\mathrm{cm/s}$. A unit timescale for the simulation can be computed as $\hat{\tau}_0 = \hat{L}_0/\hat{v}_0 = 326.4\,\mathrm{Myr}$. Note that, all the physical parameters of the simulation are suitably normalized by these scaled units.

We consider a $2D$ cylindrical grid $\{R, Z\} \in \{0, 0\}$ to $\{20\hat{L}_0, 50\hat{L}_0\}$ using 160×400 grid cells as our computational domain. The ambient medium is considered to be static initially with a constant density $\rho_m = 10^3\hat{\rho}_0$. An under-dense beam of density $\rho_j = \hat{\rho}_0$ is injected into such an ambient medium along the Z direction through a circular nozzle of unit radius $R_j = \hat{L}_0$ from the lower Z boundary. Further, a conserved tracer quantity is injected with the beam and its value is considered to separate different regions in the simulated structure, as described in more details in the following section. The injection velocity of the beam is prescribed using an initial Lorentz factor $\gamma_j = 10$.

The magnetic field is taken to be purely poloidal i.e, $\vec{B} = B_z\hat{\vec{e}}_z$ and is initially prescribed in the jet nozzle and in the ambient medium following,

$$B_z = \sqrt{2\sigma_z P_j}. \tag{3.1}$$

where, P_j is the jet pressure at $R = R_j$ estimated from the Mach number $M = v_j\sqrt{\rho_j/(\Gamma P_j) + 1/(\Gamma - 1)} = 6$ with an adiabatic index $\Gamma = 5/3$. The value for the magnetization parameter σ_z is taken to be 10^{-4} for all our simulations.

We further inject 25 Lagrangian macro-particles every two time steps so that they sample the entire jet cocoon uniformly. The macro-particles are injected with an initial power-law spectral distribution of index -9 on a γ grid spanning from $\gamma_{\min} = 1$ to $\gamma_{\max} = 10^5$ discretized with 128 bins.

The energy spectrum of the macro-particles are calculated for two different cases: (i) DSA with synchrotron, adiabatic and inverse compton (IC) losses and (ii) considering stochastic acceleration in addition to case (i). For case (i), we solve Eq. (2.1) without the

https://doi.org/10.1017/S174392132200165X Published online by Cambridge University Press

acceleration (D_A) and the diffusion (D) terms. While for case (ii), we include these terms along with the losses in the transport equation. We choose four different acceleration timescales for case (ii) to examine the influence of stochastic acceleration and turbulence damping on the emission features of the simulated jet. To clearly describe these four different scenarios we cast the acceleration timescale in the following way,

$$t_A = \frac{\tau_c(\gamma_{max}, \gamma_{min})}{\alpha} \exp\{(\tau - \tau_{inj})/\tau_d\}; \tag{3.2}$$

where $\tau_c(\gamma_{max}, \gamma_{min}) = \frac{3m_0^2c^3}{4\sigma_T[U_B(t)+U_{rad}(t)]} \left(\frac{1}{\gamma_{min}} - \frac{1}{\gamma_{max}}\right)$ is the radiative cooling time for a cosmic ray particle from γ_{max} to γ_{min} with σ_T, U_B and U_{rad} being the Thompson cross-section, magnetic and radiation field energy densities respectively. These energy densities can be computed by following $U_B = \frac{B^2}{8\pi}$ and $U_{rad} = a_{rad}T_0^4$, with a_{rad} being the radiation constant and $T_0 = 2.728\,\mathrm{K}$ being the temperature of the Cosmic Microwave Background (CMB) radiation field. $\tau_d = \eta\tau_c(\gamma_{max}, \gamma_{min})/\alpha$, we choose $\eta = 1.1$ and $\alpha = 10^4, 10^5, 10^6, 10^7$ as four different acceleration scenarios. τ_{inj} is the injection time of the Lagrangian particle in a turbulent region. For the particles that have encountered a shock, the τ_{inj} is set to be the shock hitting time, whereas, for the particles that have not crossed any shocks, the τ_{inj} is its initial injection time in the computational domain.

Moreover, for both cases we consider only the synchrotron emissivity which is calculated implicitly in the code for each Lagrangian-particle based on their local spectral distribution and interpolate it on the underlying grid (Vaidya et al. 2018).

4. Results

In this section we proceed to describe the results from our simulations. In Fig. (1), we show the synchrotron emissivity (J_ν) computed from the Lagrangian macro-particles at a frequency $\nu = 43\,GHz$ and at the time $\tau = 200\,\tau_0$ for all the test scenarios. The top left panel shows the profile of J_ν for the case when only DSA is active along with various energy losses, while all the other plots correspond to the scenario when STA is taken into account in addition to DSA. The top right panel depicts the emission profile for the case, when the turbulent acceleration timescale is calculated with $\alpha = 10^4$. For both the plots presented in the top panel, the emission structure could be seen to be very similar except at the regions where strong shocks are present (viz. along the jet spine, head and at the boundary of the cocoon), where the corresponding turbulent acceleration scenario dominates the emission. This difference is expected as the downstream region of the shock is known to be highly turbulent, thus capable of further accelerating the particles by Fermi II process, once they cross the shock. On the contrary, for the case of only DSA, once a particle crosses a shock it starts to lose its energy due to various radiative losses without any further continuous acceleration which could compensate for the energy loss. Moreover for the case of turbulent acceleration, due to the presence of the exponential term in the acceleration timescale, the energization occurs for a finite amount of time after the particle crosses the shock. This clearly imitates the turbulence damping phenomena.

The emission signatures further change as we modulate the value of α. In the lower panel of Fig. (1) the corresponding emission profiles are presented for $\alpha = 10^5, 10^6$ and 10^7. Compared to the $\alpha = 10^4$ run, all the plots in the bottom panel show a significant enhancement in the emission. This is expected, as an increase in α value manifests itself by reducing τ_A (see Eqs. (2.2) and (3.2)). Also note that, when compared to the only shock acceleration scenario (top left plot of Fig. (1)), the emission profiles in the bottom panel show a gradual enhancement in the emission from the back-flow region of the jet cocoon, which is expected to be turbulent in nature (Matthews et al. 2019), as α increases.

https://doi.org/10.1017/S174392132200165X Published online by Cambridge University Press

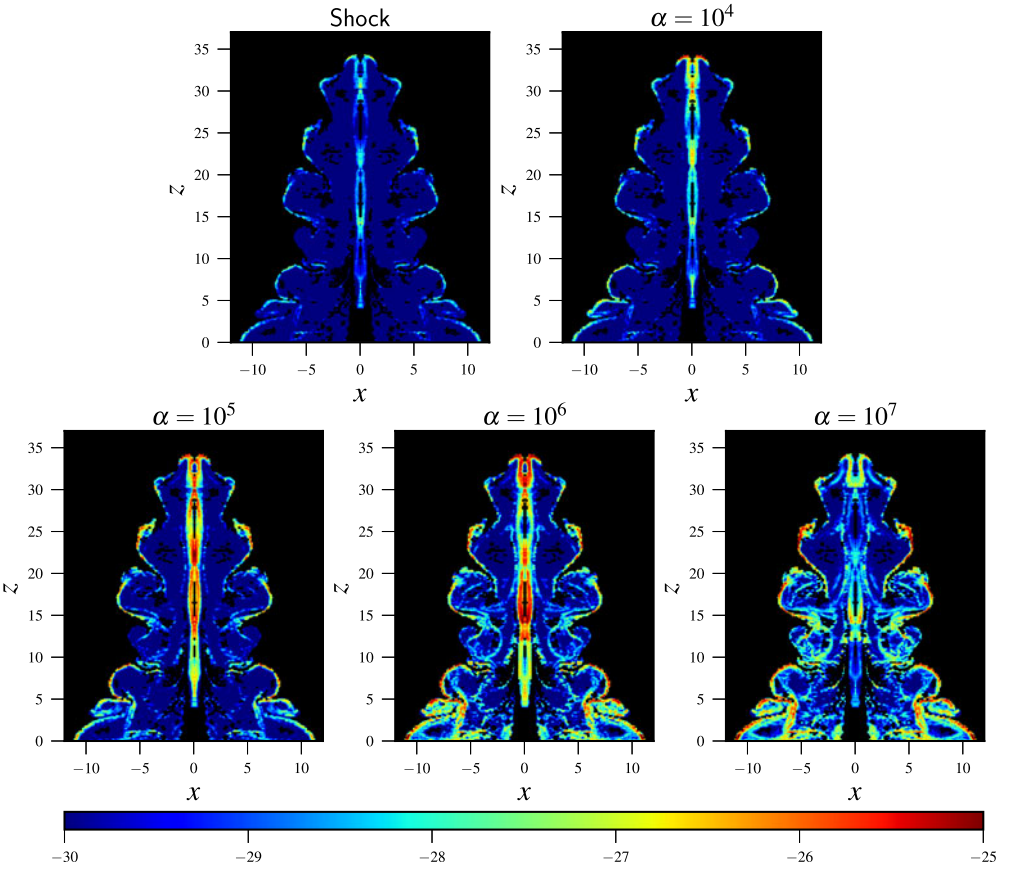

Figure 1. Emission profiles of the simulated RMHD jet, with various acceleration scenarios. *Top left:* Emission structure is shown when only DSA is considered, and all the other profiles correspond to stochastic acceleration with different values of α. The color-bar shown below corresponds to the value of emissivity in units of $erg\,s^{-1}\,cm^{-3}\,Hz^{-1}\,str^{-1}$ in logarithmic scale.

Further, observe that for both the cases with $\alpha = 10^5$ and 10^6, the emission from the jet spine region are more enhanced compared to $\alpha = 10^7$. While on the contrary, in the region inside the cocoon where weak shocks are present, the emission is more dominated for the the latter one. To analyze this phenomena in more detail, we show the magnetic field $B = \sqrt{B_r^2 + B_z^2}$ map for time $\tau = 200\tau_0$ in Fig. (2), where one can observe an order of magnitude higher value of the magnetic field in the jet spine region compared to the jet cocoon. For further quantification, we have calculated the mean magnetic field strength, weighted with the tracer, at the jet spine and in the cocoon region at time $\tau = 200\,\tau_0$. To implement this we consider tracer values > 0.8 and < 0.8 to account for the jet spine and the jet cocoon region respectively (Mukherjee et al. 2021). As expected, we find an order of magnitude higher value of the mean magnetic field in the spine region ($\approx 288\,\mu G$) compared to the cocoon region ($\approx 21\,\mu G$). With the mean magnetic field strength for both the regions, we proceed to calculate the turbulent acceleration timescale. The acceleration timescales are calculated relative to the cooling timescale $\tau_c(\gamma_{max}, \gamma_{min})$, considering the mean $\vec{B}$ field (tracer weighted) from the entire computational domain. Further to show the dependence of the acceleration timescale on different α values, we plot the variation of $\log_{10}(t_A)$, with $\log_{10}(\alpha)$ in Fig. (3) for the two different regions. We observe that,

https://doi.org/10.1017/S174392132200165X Published online by Cambridge University Press

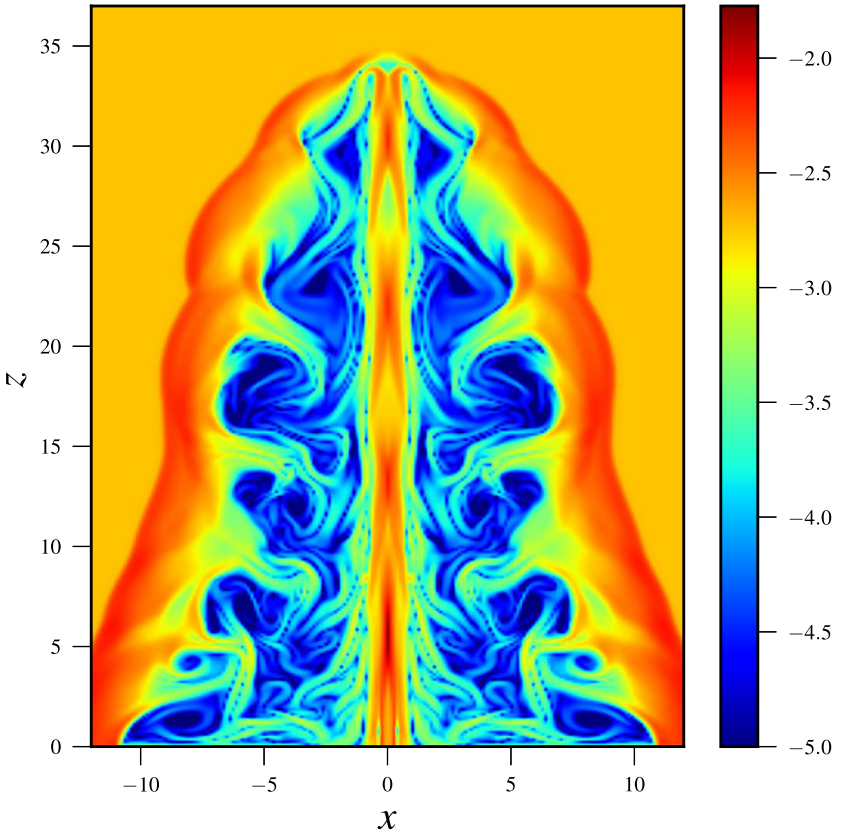

Figure 2. Normalized magnetic field map (B/B_0) of the simulated relativistic AGN jet. The color-bar shows a logarithmic scale of B/B_0. The value of the unit magnetic field being $B_0 = 1.374 \times 10^{-1}$ G.

initially in the jet spine region the timescale decays with increasing α until α reaches a critical point, $\alpha = \alpha_{jc} = 10^6$. Beyond this point the timescale increases exponentially. Due this particular behaviour of the acceleration timescale, from Fig (3) one could observe an order of magnitude increment in t_A as one moves from $\alpha = 10^6$ to $\alpha = 10^7$, in the jet spine region, thereby implying a faster acceleration for $\alpha = 10^6$. A similar functional behaviour of the timescale could be observed in the cocoon region as well. From Fig. (3) it can also be seen that in the cocoon region $\alpha = 10^7$ provides a faster turbulent acceleration compared to $\alpha = 10^6$ and below.

In summary we can say that, as the macro-particles are injected in the computational domain, the particles encounter shocks while moving along the jet spine and proceed to the turbulent downstream region. In the downstream region, due to the presence of higher magnetic field, turbulent acceleration with $\alpha = 10^6$ provides faster acceleration compared to $\alpha = 10^7$. This implies radiative losses are more dominant for $\alpha = 10^7$, in the spine region, therefore a lower emission is expected. Subsequently, as the macro-particles move into the cocoon region, due to the presence of weak shocks, the particles advect into the turbulent downstream and because of comparatively lower magnetic field than the spine region, $\alpha = 10^7$ leads to more efficient acceleration than $\alpha = 10^6$ case.

https://doi.org/10.1017/S174392132200165X Published online by Cambridge University Press

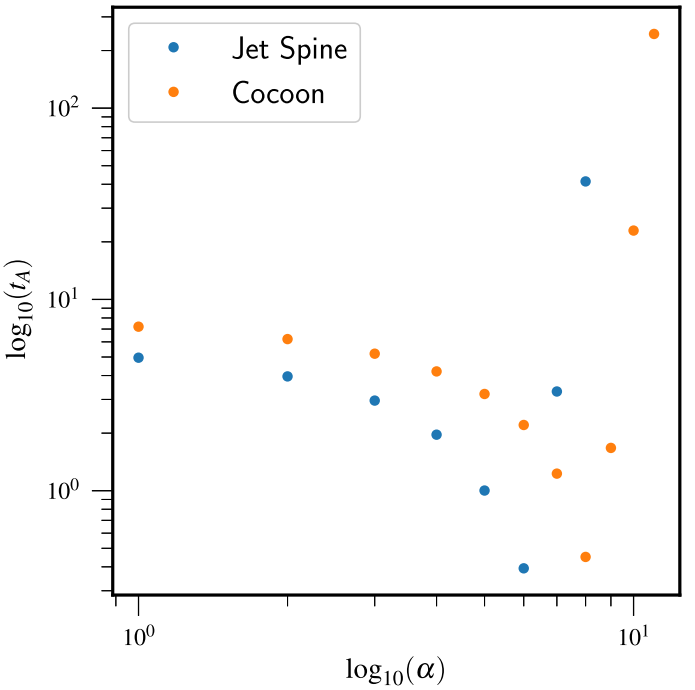

Figure 3. Dependence of (t_A) on various α values, with t_A being the turbulent acceleration timescale for both the regions, jet spine and jet cocoon.

5. Summary

Astrophysical systems provide a playground for various complex physical processes. Among them particle acceleration processes play a fundamental role in shaping the emission features observed in these systems. In this work we focus on studying the interplay of various particle acceleration processes and their effect on the emission structure of astrophysical sources. In particular, we consider a stochastic acceleration timescale, which has the ability to mimic turbulence damping phenomena. Such phenomena could be observed in various realistic turbulent environments. We have demonstrated the effect of this damping on the emission profile of synthetic astrophysical objects by analyzing a RMHD jet simulation as a toy problem. We also present a parametric study on the stochastic acceleration timescale and showed that, due to the presence of exponential damping, the stochastic acceleration could lead to a region based enhancement in the emission.

Acknowledgement

The authors express their gratitude to the referee for the insightful remarks and suggestions on the work. The authors appreciate the financial assistance provided by the Max Planck partner group award at the Indian Institute of Technology, Indore. All the simulations have been carried out using the computing facility at Indian Institute of Technology, Indore and Max Planck Gesellschaft(MPG) super-computing resources. SK would also like to thank Arghyadeep Paul, Sarvesh Mangla, Sriyasriti Acharya, Suchismita Banerjee and Yoshini Bailung for the valuable discussion sessions during the course of this work.

References

Matthews J. H., Bell A. R., Araudo A. T., Blundell K. M., 2019, EPJWC, 210, 04002. doi:10.1051/epjconf/201921004002
Fraschetti F., Giacalone J., 2012, ApJ, 755, 114. doi:10.1088/0004-637X/755/2/114
Hanasz M., Strong A. W., Girichidis P., 2021, LRCA, 7, 2. doi:10.1007/s41115-021-00011-1
Winner G., Pfrommer C., Girichidis P., Pakmor R., 2019, MNRAS, 488, 2235. doi:10.1093/mnras/stz1792
Vazza F., Wittor D., Brunetti G., Brüggen M., 2021, A&A, 653, A23. doi:10.1051/0004-6361/202140513
Petrosian V., 2012, SSRv, 173, 535. doi:10.1007/s11214-012-9900-6
Vurm I., Poutanen J., 2009, ApJ, 698, 293. doi:10.1088/0004-637X/698/1/293
Ferrand G., Marcowith A., 2010, A&A, 510, A101. doi:10.1051/0004-6361/200913520
Schlickeiser R., Dermer C. D., 2000, A&A, 360, 789
O'Sullivan S., Reville B., Taylor A. M., 2009, MNRAS, 400, 248. doi:10.1111/j.1365-2966.2009.15442.x
Fan Z.-H., Liu S., Wang J.-M., Fryer C. L., Li H., 2008, ApJL, 673, L139. doi:10.1086/528372
Donnert J., Brunetti G., 2014, MNRAS, 443, 3564. doi:10.1093/mnras/stu1417
Asano K., Hayashida M., 2018, ApJ, 861, 31. doi:10.3847/1538-4357/aac82a
Blandford R. D., 1994, ApJS, 90, 515. doi:10.1086/191869
Marcowith A., Ferrand G., Grech M., Meliani Z., Plotnikov I., Walder R., 2020, LRCA, 6, 1. doi:10.1007/s41115-020-0007-6
Webb G. M., 1989, ApJ, 340, 1112. doi:10.1086/167462
Fermi E., 1949, PhRv, 75, 1169. doi:10.1103/PhysRev.75.1169
Vaidya B., Mignone A., Bodo G., Rossi P., Massaglia S., 2018, ApJ, 865, 144. doi:10.3847/1538-4357/aadd17
Kundu S., Vaidya B., Mignone A., 2021, ApJ, 921, 74. doi:10.3847/1538-4357/ac1ba5
Mukherjee D., Bodo G., Rossi P., Mignone A., Vaidya B., 2021, MNRAS, 505, 2267. doi:10.1093/mnras/stab1327
Brunetti G., Lazarian A., 2007, MNRAS, 378, 245. doi:10.1111/j.1365-2966.2007.11771.x
Schlickeiser R., 2002, cra.book
Mignone A., Bodo G., Massaglia S., Matsakos T., Tesileanu O., Zanni C., Ferrari A., 2007, ApJS, 170, 228. doi:10.1086/513316

Discussion

TOMOYUKI: Has the coefficient of diffusion for the particle acceleration been calculated from the MHD simulation?

SAYAN: Yes, it has been calculated from the MHD simulation. The simulation gave the value of the magnetic field at each points on the grid and we calculate the diffusion coefficient from that. We also consider the dependence of the diffusion coefficient on the particle Lorentz factor as $D \propto \gamma^2$.